



Research Article

Observation System Optimization of Offshore Acoustic Exploration for Estimating Submarine Geological Structures via Directivity Analysis

Chao Fu ¹, Lei Hao,¹ Pengfei Zhou,² Lei Chen ¹, Xiaobin Xu,² Kai Wang,² and Miaojun Sun³

¹Geotechnical and Structural Engineering Research Center, Shandong University, Jinan 250061, China

²Shandong Hi-speed Group Co., Ltd., Jinan 250101, China

³Huadong Engineering Co., Ltd., Zhejiang 311122, China

Correspondence should be addressed to Lei Chen; clei667@163.com

Received 20 March 2022; Accepted 28 April 2022; Published 15 July 2022

Academic Editor: Jianyong Han

Copyright © 2022 Chao Fu et al. This is an open access article distributed under the Creative Commons Attribution License, which permits unrestricted use, distribution, and reproduction in any medium, provided the original work is properly cited.

To better understand the shallow sea geological information and avoid the risk caused by potential geo-disasters, the efficient offshore geological exploration methods are required. Better detection resolution can be obtained by using a spark source. As the foundation, the observation system plays an important role for geological detection. The influence of the variation of the parameters of the observation system on the detection accuracy is analysed theoretically. Then, the numerical simulations based on the finite difference method was applied, and imaging characteristics of observation system with different parameter were studied. For submarine acoustic exploration, the spark source with frequency over 200 Hz can obtain the clear reflections for geological interpretation; besides, the receiver array with the interval of 5 m–10 m helps to obtain better wave signals when the buried depth of a geological body is less than 300 m, and the width is more than 10 m. Based on numerical simulations, the observation system was optimized and designed. The results of numerical examples show that the accurate position information of the structure can be obtained by using the observation system proposed in this paper. Different imaging performances are obtained by adjusting the parameters of the observation system. On this basis, combined with directivity analysis, the optimal observation system parameters are proposed. Finally, the proposed observation system is used to image the fault model. The research results of this paper can provide reference for the observation system design in similar projects.

1. Introduction

With the rapid development of social economy, the resources and living space are required urgently [1]. Rational utilization of offshore resources and protection of the marine environment are important strategies [2]. In recent years, the rapid development of marine resources (such as oil and gas) and offshore engineering (such as cross-sea bridges and subsea tunnels) has led to a growing concern on the marine geological environment [3]. Marine geo-disasters (such as submarine landslides and submarine faults) enormously threaten and often destroy the offshore engineering [4]. For example, in 1969, Hurricane Camille induced a submarine landslide, and the fast-moving landslide body destroyed three offshore platforms (loss over one million dollars) [5].

Therefore, accurate geological detection and warning on geo-hazards risk in time are critical to the safety of offshore engineering [6].

At present, the traditional methods [7] mainly include echo sounding systems [8, 9], side sonar systems [10–13], shallow profile systems, and high-resolution seismic detection systems [14]. In practice, the detection of marine geo-disasters is often based on the combination of seabed topography and various means of detection [15, 16]. Among them, acoustic exploration has been widely used [17]. Research on the detection of marine geo-disasters has been the core of marine geologists [18]. Many researchers have done a lot of work for them, such as OOI (the Ocean Observatories Initiative) program and the DONET (Development of Dense Ocean-floor Network System for Earthquake and Tsunami)

systems in Japan, as well as the ESONET (the European Sea Observatory Network) system and the COSTA (Continental Slope Stability) program [19–21]. These research works promoted the progress in the formation mechanism of marine geo-disasters and detection techniques [22]. However, for the specific environment and requirement, the observation system and processing approach should be optimized for the best result, improving the accuracy of geological interpretation (depth less than 300 m, width greater than 10 m).

This method is suitable for the detection in the offshore and seabed engineering survey period. The observation system can be adaptively adjusted according to the difference of underground geological disaster, and the fault can be imaged with higher resolution. The remainder of the paper was organized as follows. First, combined with engineering requirements, we propose an optimization method for the observation system under the condition of array reception. Then, based on the imaging results, different parameters are evaluated by the observation system evaluation method, and the optimal observation parameters are obtained. Finally, the optimized observation system parameters are used for data processing and imaging. Numerical model examples show that the directivity parameter is a valid method for evaluating the observation system and can obtain the exact position of the interface.

2. Observation System and Methodology

The observation system is the key foundation for exploration. A better observation system can effectively improve the exploration result. For acoustic exploration, the key factors are the source and receiver array. We used the acoustic directivity parameter to initially evaluate the observation system. The directivity parameter can be expressed as follows:

$$F_{\theta}(\alpha) = \frac{|\sin[N\pi fd/v(\sin\alpha - \sin\theta)]|}{|N \sin[\pi fd/v(\sin\alpha - \sin\theta)]|}, \quad (1)$$

where N represents the number of sources, f represents the dominant frequency of source, d represents the source spacing, v represents the medium velocity, and α represents the scanning angle, $\alpha \in [-\pi/2, \pi/2]$. θ is the special angle. In this manuscript, it is equal to 90. With the increase of the number of sources or geophones, the detection effect will be improved. However, it will reduce the detection efficiency and improve the cost. Therefore, we use the ratio of the side lobe to main lobe of the directivity parameter as the criterion. When the side lobe ratio is higher than 0.6, we think the detection effect is higher.

2.1. Main Parameters of the Observation System. The typical sources for acoustic exploration are the air gun and spark. The main parameter is frequency. Frequency determines the depth and the resolution of the migration result. In general, the high frequency wavelet has a better resolution. However, the attenuation of the high frequency is larger than that of the lower frequency signal, resulting in a shallower detection

depth [23]. The detection demand of landslides along the offshore is no more than 200 m, and the detection target scale is about 10 m. Therefore, we choose the high frequency spark source as the excitation signal.

The geophone interval of the receiver array. The geophone interval of the receiver array is the basic parameter of the observation system, relating to the resolution and the coverage of acoustic exploration. In general, the observation system (including the source and receivers) is placed under the sea surface. The following principles should be met [24]: firstly, the track pitch should be smaller than the first Fresnel zone; secondly, the track pitch should satisfy the sampling theorem to avoid spatial aliasing; thirdly, the application cost should be minimum.

To reveal the imaging characteristics of the receiver array with different intervals, the numerical simulations and directivity analysis are introduced to evaluate the observation system. In simulation, the total number of sources is 20. Four geophone intervals are adopted by 2 m, 5 m, 10 m, and 20 m, and the total number of corresponding geophones are 251, 101, 51, and 26. The sampling rate is 0.5 ms, and the Ricker wavelet of 200 Hz is adopted.

2.2. Numerical Simulation Method. The typical acoustic numerical modelling method includes a geometric ray and wave equation. The wave equation method is better at simulating the seismic propagation in complex geological models. In this study, the finite difference method based on the two-dimensional wave equation is adopted. For two-dimensional models, the wave equation is as follows:

$$\frac{\partial^2 U(x, z)}{\partial x^2} + \frac{\partial^2 U(x, z)}{\partial z^2} = \frac{1}{V(x, z)^2} \frac{\partial^2 U(x, z)}{\partial t^2} + s(x, z, t), \quad (2)$$

where $V(x, z)$ represents the velocity in the vertical direction of the particle at (x, z) ; U represents pressure field; and $s(x, z, t)$ represents the source function. In the acoustic wave equation, the properties of the medium are usually designed by wave velocity $V(x, z)$. Then, the equation can be transferred based on the Taylor formula, and the equation of high-order finite difference is as follows [25]:

$$\begin{aligned} & U_{i,j}^{n+1} - 2U_{i,j}^n + U_{i,j}^{n-1} \\ &= V_{i,j}^2 \cdot \Delta t^2 \\ & \cdot \left(\frac{U_{i+m,j}^n - 2U_{i,j}^n + U_{i-m,j}^n}{\Delta x^2} + \frac{U_{i,j+m}^n - 2U_{i,j}^n + U_{i,j-m}^n}{\Delta z^2} \right). \end{aligned} \quad (3)$$

2.3. Data Processing Method. To compare observation systems with different parameters, the seismic data are processed for imaging the geological condition. The processing scheme mainly consists of three parts: preprocessing, waveform processing, and imaging. To obtain more accurate imaging, we use Gaussian smoothing (window size equal to

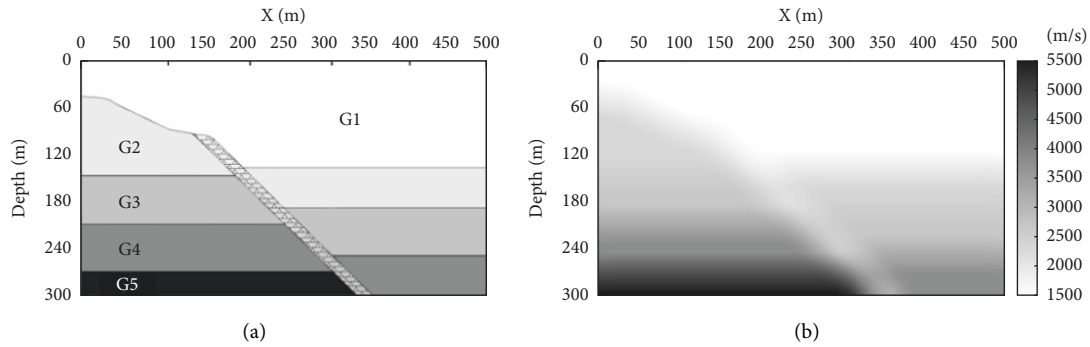


FIGURE 1: The submarine geological model with layered media and an inclined fault. (a) True velocity model. (b) Initial velocity model for imaging.

10) for the initial model to obtain the model after imaging. The preprocessing includes data conversion. The waveform processing mainly includes direct wave removing, attenuation compensation, spectrum analysis, amplitude balance, generate common middle point (CMP) gather, velocity analysis, and normal moveout (NMO) correction. Meanwhile, the filtering method is used to extract effective signals and remove noise in reflected waves [26–28]. In addition, the imaging method includes stack, Kirchhoff poststack migration [29], and time-depth conversion.

3. Numerical Examples

To design and optimize the parameters of the observation system, a submarine geological model with a fault was built and studied as an example. As is shown in Figure 1(a), the model has the length of 500 m with the depth of 300 m. The first layer which marked G1 represents the seawater. The inclined fault is located at the middle of the geological model. The bedrock is composed by 3 or 4 layers. The geological parameters of G1 are $V_p=1500$ m/s. The geological parameters of G2 are $V_p=2200$ m/s. The geological parameters of G3 are $V_p=2500$ m/s. The geological parameters of G4 are $V_p=3500$ m/s. The geological parameters of G5 are $V_p=5500$ m/s. The fault is filled by broken rocks and water. Therefore, the wave speed of V_p is 1700 m/s. To obtain more accurate imaging, we use Gaussian smoothing for the initial model (Figure 1(a)) to obtain the model after imaging (Figure 1(b)). In practice, the velocity can be obtained by velocity scanning or tomography imaging method calculations.

3.1. Imaging Difference of the Observation System Using the Wavelet with Different Frequencies. At first, the influence of wavelet frequency on the imaging result was studied. To study the difference, the same receiver array with the geophone interval of 5 m and the source with the wave spreading around were adopted. Meanwhile, the common source gather (CSG) mode with one source was adopted in data acquisition. Figure 2 shows the imaging results in time domain using the wavelet with the frequency of 50 Hz, 100 Hz, 200 Hz, and 400 Hz.

According to the imaging results, it is easy to find that the wavelength of these four results are different. Figure 2(a)

is the imaging result using the wavelet with the frequency of 50 Hz, which shows the reflected waves have the length of about 40 m. In that case, the boundary between the seabed and the stratum of the large scale (A1) can be basically displayed, but the fractured zone in the middle is blurred (A2). Although the existence of interfaces (A1) can be judged, it is hard to accurately locate the interfaces. Figure 2(b) is the imaging result using the wavelet with the frequency of 100 Hz, which shows the clearer reflected waves with the increasing frequency. In that case, the wavelength is about 20 m, and the existence of the fracture zone (B1) can be judged. Figure 2(c) is the result using the wavelet with the frequency of 200 Hz, the image is the clearest, and the boundary and the thickness (C1) are easily estimated. Figure 2(d) is the result using the wavelet with the frequency of 400 Hz, and the wavelet length is the smallest of all. However, when the high-frequency wave propagates in the stratum, the energy of the reflected signal is weaker (D2). The interface position is obtained for both 200 Hz and 400 Hz frequency wavelets. However, when the frequency is 400 Hz, the energy of the event is obviously weakened, and the imaging sharpness is decreased. As the frequency increases, the artifacts in the imaging results become more and more significant. Moreover, the acoustic waves are attenuated, and the low frequencies excited by the spark source are more stable. Combining the above information, we finally chose the 200 Hz frequency as the excitation frequency.

3.2. Imaging Difference of the Observation System with Different Geophone Intervals. It is necessary to set the geophone interval reasonably for imaging resolution. According to the theoretical analysis, the geophone interval has influence on the coverage time and imaging result, as well as the detection cost. In that case, finding the maximum geophone interval (meeting the resolution requirement) is important to field exploration. In this part, the receiver arrays with different geophone intervals were studied, respectively.

Figure 3 shows the imaging results using the observation system with different intervals (2 m, 5 m, 10 m, and 20 m, respectively) as well as direction analysis (the greater the energy in a certain direction, the stronger the directivity). When the pointing distribution is uniform, it indicates that the acoustic wave beam has more balanced illumination in

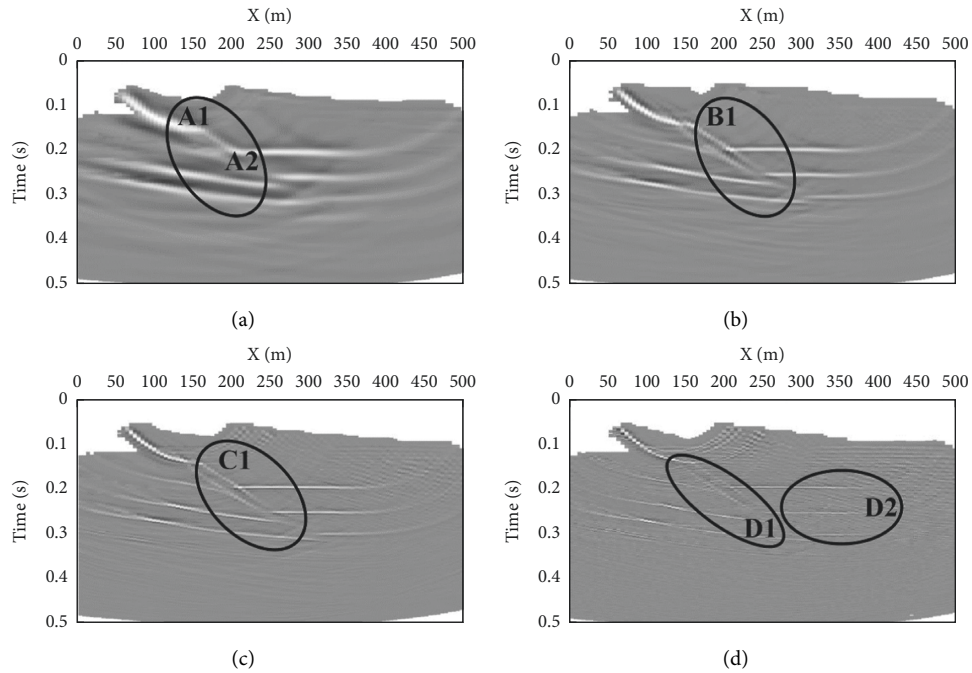


FIGURE 2: The imaging results in time domain using the wavelet with different frequencies: (a) imaging result of 50 Hz, (b) imaging result of 100 Hz, (c) imaging result of 200 Hz, and (d) imaging result of 400 Hz.

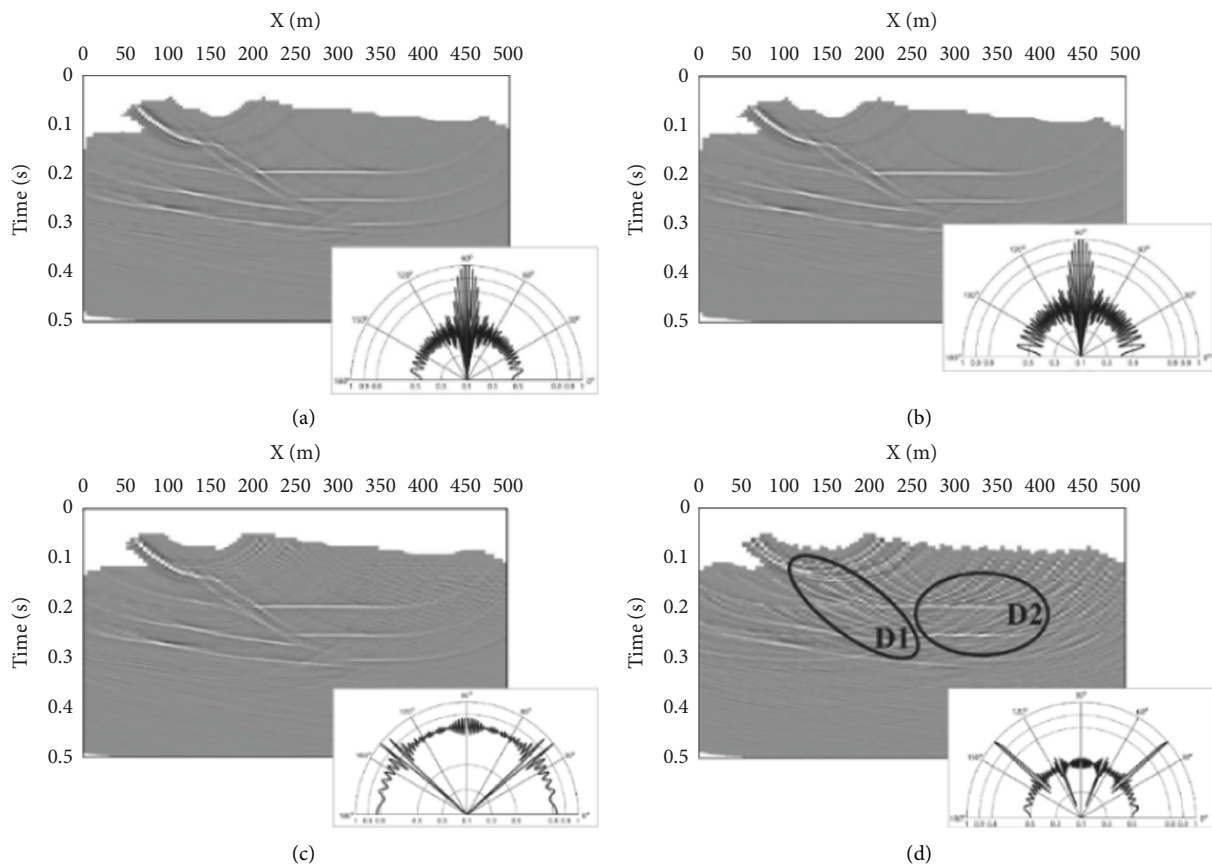


FIGURE 3: The imaging results in time domain using the receiver array with different geophone intervals: (a) the receiver array with the geophone interval of 2 m. (b) The receiver array with the geophone interval of 5 m. (c) The receiver array with the geophone interval of 10 m and (d) the receiver array with the geophone interval of 20 m.

all directions). Figure 3(a) is the imaging result using the observation array with the geophone interval of 2 m, in which the reflected waves of interfaces are clearly imaged. Figure 3(b) is the imaging result with the geophone interval of 5 m, and the position of interface can also be recognized. However, the resolution reduces when the geophone interval increases. Figure 3(c) is the imaging result with the geophone interval of 10 m, and the resolution of the stratum is further decreased. Meanwhile, the resolution is improved with the increasing depth. Figure 3(d) is the imaging result with the geophone interval of 20 m, and it is hard to recognize the reflected waves by interfaces (especially for the reflected waves of faults). In total, in the depth of 300 m range, 200 Hz acoustic wave can achieve better imaging results. The smaller the geophone interval, the greater the total number of geophones. Therefore, there are fewer artifacts. In the premise of ensuring the quality of imaging, we want to have less number of geophones, geophone interval of 2 m, 5 m is less imaging artifacts, but the number of geophones is too much (250, 100, respectively). With an interval of 20, although the number of geophones is less (25), it produces many artifacts that interfere with the identification of anomalies. In contrast, when the geophone interval is 10 m, the artifacts have a little effect on the anomaly identification. And the geophone data are relatively small (50), so the geophone interval range is from 5 m to 10 m.

The directivity of the wave field obtained by Figures 3(a) and 3(b) is clearer, and the direction of 90 degrees is stronger, indicating that most of the energy is incident into the medium perpendicular to the sea level. This is beneficial to receive more reflected artifact information. In addition, the channel with the spacing of 5 m (Figure 3(b)) requires fewer geophones to achieve the similar result, which is better to the massive data acquisition. Figure 3(c) shows two sharp peaks at 45 degrees and 135 degrees, which means that the sound waves are pointing and diverging. It can be clearly seen from the imaging results that many artifacts are produced. It is inconvenient for the identification of faults. Therefore, the source with the dominate frequency of 200 Hz and the geophone with the interval of 5 m to 10 m are chosen for this study.

3.3. Observation System for Submarine Acoustic Exploration.

According to the requirements of offshore geological exploration (the general depth of detection is 300 m) and the theoretical analysis above, an observation system suitable for offshore geological acoustic exploration is designed: (1) the propagation of the source should be mainly in the vertical direction to obtain clearer events. Meanwhile, the source should be placed under the depth of 5 m or more of sea level to couple the medium; (2) the frequency of the source could be 200 Hz to obtain high-resolution imaging of submarine structures; (3) the geophone interval of the receiver array should be 5–10 m to obtain continuous reflections of submarine structures.

Based on the parameters above, the imaging result in depth domain was carried out (Figure 4). The result shows that the estimated reflected waves of interfaces agree with the

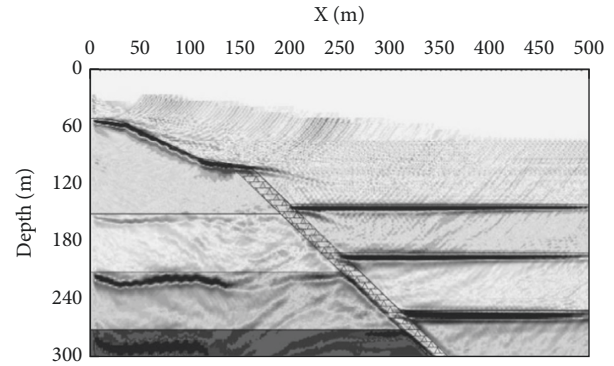


FIGURE 4: The imaging result in depth domain using the designed observation system.

interfaces in the geological model. Meanwhile, the thickness of the fault could be estimated according to the break point of reflected waves.

4. Verification and Discussion

4.1. Numerical Verification. For submarine geological condition, there are more than 20 kinds of geo-disasters that can cause damage and threaten engineering safety [30]. In general, the most dangerous geo-disasters are submarine faults and landslides. To further examine the feasibility of the designed observation system, three geological models with typical adverse geologies (submarine landslides and submarine faults) were built, and the numerical simulations were conducted. Figure 5 shows the numerical simulation of submarine landslides and submarine faults. The optimized observation system was adopted to obtain seismic signals.

Figure 5(a) shows the numerical simulation of submarine landslides. Figure 5(b) shows the migration result in time domain, which indicates three interfaces under the seawater. To better realize the location, the time-depth conversion was adopted (Figure 5(c)). The submarine bedrock interface and the submarine landslide surfaces could be estimated, and the locations are consistent with the actual model.

To further verify the designed observation system, a geological model with multilayers was built (consists of six layers and an inclined fault). As Figure 5(d) shows, six layers are placed horizontally with an inclined fault. The fault has the thickness of 20 m. Figure 5(e) shows the migration result in time domain, which shows six interfaces under the sea level. However, the reflected waves of second horizontal interfaces are blurry due to the low difference of wave impedance on the two sides of this interface. Meanwhile, two reflected waves by the fault can be recognized obviously. Then, the time-depth conversion was adopted to get the location of geological interfaces (Figure 5(f)). In depth domain, the estimated layers interfaces and fault boundaries are consistent with the actual model. Meanwhile, with the number of layers increasing, the reflected waves of deep interfaces become blurry due to the multiples.

Figure 5(g) is the numerical simulation by using the geological model with six layers and two inclined faults. The

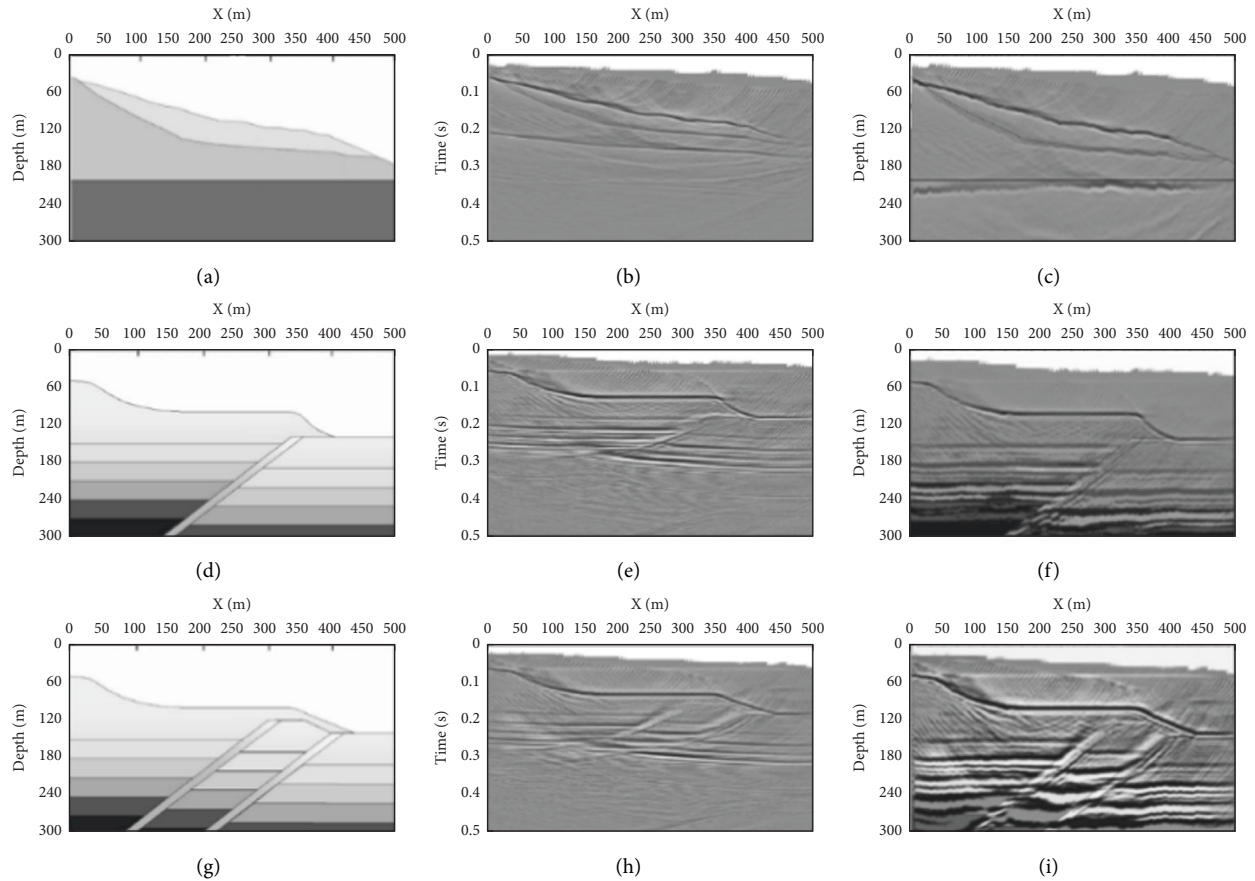


FIGURE 5: The numerical experiments: (a), (b), and (c) are the geological model, imaging in time domain, and imaging in depth domain of the submarine landslide, respectively; (d), (e), and (f) are the geological model, imaging in time domain, and imaging in depth domain of the submarine fault (single), respectively; (g), (h), and (i) are the geological model, imaging in time domain, and imaging in depth domain of the submarine fault (double), respectively.

two faults are parallel to each other and have the distance of 100 m in the horizontal direction. Figure 5(h) is the migration result in time domain, which shows the six interfaces under the seawater and two inclined interfaces. Due to the reason that velocity of layer increases with the increasing depth and the fault has lower velocity, the reflected wave by the interface under the fault are bent in time domain. Meanwhile, the thickness of faults could be recognized roughly. Then, the time-depth conversion was adopted to get the migration result in depth domain (Figure 5(i)). The result shows that the estimated layers interfaces and fault boundaries are consistent with the actual model.

5. Discussion

To optimize the observation system and support the imaging result of submarine geological structures, the main parameters of the observation system (the source frequency and geophone interval of the receiver array) were studied. The influence characteristics of the main parameters are as follows:

(1) The dominate frequency of the source has a great influence on the detection accuracy and imaging. Compared to the source with the dominate

frequency of 30 Hz (explosion source), the frequency of the air gun or spark source in the ocean is higher and helps to improve the resolution of geological conditions (especially for offshore landslides or faults). To balance the detection depth and resolution, the frequency of the source should be 200 Hz for offshore acoustic exploration. In order to improve the performance of imaging, data processing and imaging also need to be implemented. For example, random noise or regular noise attenuation and least-squares reverse time migration (RTM).

- (2) In this manuscript, we assume that the medium is relatively intact; however, there is an attenuation of acoustic waves in the broken medium which is not negligible. Due to the attenuation of acoustic waves, the detection depth and imaging accuracy are reduced. For this problem, the Q-RTM can be introduced to solve it, and this will be our next step to study.
- (3) The directivity parameter of phased array ultrasound is introduced to evaluate the performance of the observation system. For the geophone interval of the receiver array, the imaging test results show that the imaging result improves with the decreasing

geophone interval. Considering the detection cost, the geophone interval should be in the range from 5 m to 10 m. It should be noted that this observation system evaluation method can be used in other fields, such as ultrasonic structural health detection (SHD), array sonic ahead prediction (ASAP), and physical model on the digital ultrasonic system (PMDUS).

6. Conclusion

The observation system is the important foundation for acoustic detection. In this paper, we designed an observation system and analysed the imaging characteristics by this system.

- (1) The main parameters of offshore acoustic detection are analysed. Based on the numerical simulation, the influence characteristics of different observation parameters are studied systematically. The theoretical analysis indicates a suitable frequency (200 Hz) and receiver interval (5 m–10 m) for offshore acoustic exploration when the geo-disasters are 300 m below the water surface. Then, an observation system for offshore acoustic exploration has been designed.
- (2) Based on numerical simulation, the feasibility of the designed observation system was fully verified based on the geological model with typical adverse geologies (submarine landslides and submarine faults). When determining the parameters of the observation system using a numerical model, the imaging quality of the target depth can be used to determine. The migration result shows that the designed observation system helps to recognize the multi-interfaces and locate the position.

In the next research, the applicability of the designed observation system for submarine exploration using a passive source should be further studied. Meanwhile, the full waveform inversion is another research key point for accurately examining the velocity for imaging the geological conditions under the seabed.

Data Availability

The original data used to support the findings of this study may be released upon application to the corresponding author who can be contacted at clei667@163.com.

Conflicts of Interest

The authors declare that they have no conflicts of interest.

Acknowledgments

The research was supported by the Science & Technology Program of Department of Transport of Shandong Province (2019B47_2), the National Natural Science Foundation of China (42107165), Natural Science Fund project in Shandong province (ZR2021QE242), and Science and

Technology Research and Development Plan of China National Railway Group Co., Ltd (P2019G038).

References

- [1] J. Zhang and M. Zhao, "Monitoring system for circular deformation in metro shield tunnels in soft soils," *Advances in Civil Engineering*, vol. 2020, pp. 1–12, 2020.
- [2] Z. Zhu and C. Yan, "Detection of offshore submarine faults based on shallow seismic exploration technology," *The Journal of Geology*, vol. 39, no. 2, pp. 258–262, 2015.
- [3] X. Cheng, G. Li, J. Chen, K. Zhang, and X. Du, "Seismic response of a submarine tunnel under the action of a sea wave," *Marine Structures*, vol. 60, pp. 122–135, 2018.
- [4] J. Frey-Martínez, J. Cartwright, and D. James, "Frontally confined versus frontally emergent submarine landslides: a 3D seismic characterisation," *Marine and Petroleum Geology*, vol. 23, no. 5, pp. 585–604, 2006.
- [5] G. P. Williams and H. P. Guy, *Erosional and Depositional Aspects of Hurricane Camille in Virginia*, US Government Printing Office, 1973.
- [6] K. A. Weitemeyer, A. M. Tréhu, and A. M. Tréhu, "A marine electromagnetic survey to detect gas hydrate at Hydrate Ridge, Oregon," *Geophysical Journal International*, vol. 187, no. 1, pp. 45–62, 2011.
- [7] E. Sounding, "High-resolution sub-bottom profiling using parametric acoustics," *International Ocean Systems*, vol. 7, no. 4, pp. 6–11, 2003.
- [8] D. W. Beran, W. H. Hooke, and S. F. Clifford, "Acoustic echosounding techniques and their application to gravity-wave, turbulence, and stability studies," *Boundary-Layer Meteorology*, vol. 4, no. 1, pp. 133–153, 1973.
- [9] U. Nixdorf, D. Steinhage, U. Meyer et al., "The newly developed airborne radio-echo sounding system of the AWI as a glaciological tool," *Annals of Glaciology*, vol. 29, pp. 231–238, 1999.
- [10] H. P. Johnson and M. Helferty, "The geological interpretation of side-scan sonar," *Reviews of Geophysics*, vol. 28, no. 4, pp. 357–380, 1990.
- [11] C. De Moustier and H. Matsumoto, "Seafloor acoustic remote sensing with multibeam echo-sounders and bathymetric sidescan sonar systems," *Marine Geophysical Researches*, vol. 15, no. 1, pp. 27–42, 1993.
- [12] W. H. Key, "Side scan sonar technology[C]//OCEANS 2000 MTS/IEEE Conference and Exhibition," *Conference proceedings, IEEE*, vol. 2, , pp. 1029–1033, 2000.
- [13] F. Yu, B. He, and K. Li, "Side-scan sonar images segmentation for AUV with recurrent residual convolutional neural network module and self-guidance module," *Applied Ocean Research*, vol. 113, 2021.
- [14] M. Greco and S. Watts, "Modeling and processing of radar signals for earth observation," *International Journal of Navigation and Observation*, vol. 2008, pp. 1–2, 2008.
- [15] B. G. McAdoo, L. F. Pratson, and D. L. Orange, "Submarine landslide geomorphology, US continental slope," *Marine Geology*, vol. 169, no. 1–2, pp. 103–136, 2000.
- [16] M. Canals, G. Lastras, R. Urgeles et al., "Slope failure dynamics and impacts from seafloor and shallow sub-seafloor geophysical data: case studies from the COSTA project," *Marine Geology*, vol. 213, no. 1–4, pp. 9–72, 2004.
- [17] J. L. Deichmann, A. Hernández-Serna, C. M. Delgado, M. Campos-Cerqueira, and T. M. Aide, "Soundscape analysis and acoustic monitoring document impacts of natural gas

- exploration on biodiversity in a tropical forest,” *Ecological Indicators*, vol. 74, pp. 39–48, 2017.
- [18] T. Y. Zhou and B. W. Lian, “A multipath processing technology based on multiparameter-combined observation in GNSS,” *Mobile Information Systems*, vol. 2021, no. 2021, pp. 1–11, 2021.
- [19] J. Mienert, “COSTA—continental slope stability: major aims and topics,” *Marine Geology*, vol. 1, no. 213, pp. 1–7, 2004.
- [20] Y. Osada, M. Kido, H. Fujimoto, and Y. Kaneda, “Development of a seafloor acoustic ranging system toward the seafloor cable network system,” *Ocean Engineering*, vol. 35, no. 14–15, pp. 1401–1405, 2008.
- [21] I. Puillat, R. Person, C. Leveque et al., “Standardization prospective in esonet noe and a possible implementation on the antares site,” *Nuclear Instruments and Methods in Physics Research Section A: Accelerators, Spectrometers, Detectors and Associated Equipment*, vol. 602, no. 1, pp. 240–245, 2009.
- [22] Xi Wang, T. Chen, D. Li, and S. Yu, “Processing methods for digital image data based on the geographic information system,” *Complexity*, vol. 22, 2021.
- [23] Y. Chen, S. Fomel, and J. Hu, “Iterative deblending of simultaneous-source seismic data using seislet-domain shaping regularization,” *Geophysics*, vol. 79, no. 5, pp. 179–189, 2013.
- [24] V. Cerveny, *Seismic ray Theory*, Cambridge University Press, 2005.
- [25] H. Liu, N. Dai, F. Niu, and W. Wu, “An explicit time evolution method for acoustic wave propagation,” *Geophysics*, vol. 79, no. 3, pp. T117–T124, 2014.
- [26] Y. Chen, “Deblending using a space-varying median filter,” *Exploration Geophysics*, vol. 46, no. 4, p. 5183, 2014.
- [27] B. Liu, C. Fu, Y. Ren, Q. Zhang, X. Xu, and Y. Chen, “Structural complexity-guided predictive filtering,” *Geophysical Prospecting*, vol. 68, no. 5, pp. 1509–1522, 2020.
- [28] S. Yang, Z. Wang, J. Wang et al., “Defect segmentation: mapping tunnel lining internal defects with ground penetrating radar data using a convolutional neural network,” *Construction and Building Materials*, vol. 319, 2022.
- [29] C. Oren and R. L. Nowack, “An overview of reproducible 3D seismic data processing and imaging using Madagascar,” *Geophysics*, vol. 83, no. 2, pp. F9–F20, 2018.
- [30] Y. Xue, F. Kong, S. Li et al., “Water and mud inrush hazard in underground engineering: genesis, evolution and prevention,” *Tunnelling and Underground Space Technology*, vol. 114, 2021.